

# A Novel Approach of Computer-Aided Detection of Focal Ground-Glass Opacity in 2D Lung CT image

Li Song<sup>a</sup>, Xiabi Liu<sup>a1</sup>, Ali Yang<sup>a</sup>, Kunpeng Pang<sup>a</sup>, Chunwu Zhou<sup>b</sup>, Xinming Zhao<sup>b</sup>, Yanfeng Zhao<sup>b</sup>

<sup>a</sup> Beijing Laboratory of Intelligent Information Technology, School of Computer Science and Technology, Beijing Institute of Technology, Beijing 100081, China; <sup>b</sup> Dept. of Imaging Diagnosis, Cancer Hospital, Chinese Academy of Medical Sciences, Beijing, China

## ABSTRACT

Focal Ground-Glass Opacity (fGGO) plays an important role in diagnose of lung cancers. This paper proposes a novel approach for detecting fGGOs in 2D lung CT images. The approach consists of two stages: extracting regions of interests (ROIs) and labeling each ROI as fGGO or non-fGGO. In the first stage, we use the techniques of Otsu thresholding and mathematical morphology to segment lung parenchyma from lung CT images and extract ROIs in lung parenchyma. In the second stage, a Bayesian classifier is constructed based on the Gaussian mixture Modeling (GMM) of the distribution of visual features of fGGOs to fulfill ROI identification. The parameters in the classifier are estimated from training data by the discriminative learning method of Max-Min posterior Pseudo-probabilities (MMP). A genetic algorithm is further developed to select compact and discriminative features for the classifier. We evaluated the proposed fGGO detection approach through 5-fold cross-validation experiments on a set of 69 lung CT scans that contain 70 fGGOs. The proposed approach achieves the detection sensitivity of 85.7% at the false positive rate of 2.5 per scan, which proves its effectiveness. We also demonstrate the usefulness of our genetic algorithm based feature selection method and MMP discriminative learning method through comparing them with without-selection strategy and Support Vector Machines (SVMs), respectively, in the experiments.

**Keywords:** lung CT images, focal ground-glass opacity (fGGO) detection, lung parenchyma segmentation, extraction of region of interests (ROI), imaging sign classification

## 1. INTRODUCTION

Ground-glass opacity (GGO) is defined as a hazy increase in lung attenuation without obscuration of underlying vascular markings [1], and can be divided into two categories: diffuse GGO and focal GGO (fGGO). The diffuse GGO is defined as a homogeneous opacification in which normal anatomical detail of the lung are still visible but giving a hazy appearance to the lung fields [2]. The focal GGO can be considered as the isolated and small region of GGO, and can also be called localized GGO or ground-glass nodule. The fGGO plays an important role in diagnose of lung cancer. Data from many studies suggests that the fGGO is a finding of early adenocarcinoma [3] or could be an early sign of localized bronchioloalveolar carcinoma (BAC) [4]. However, due to their indistinct boundaries and similarity to its surrounding structures, the labeling of fGGO is time- and labor-consuming or even difficult for radiologists. So it has attracted the interests of researchers in recent years to automatically detect fGGOs in lung CT images for aiding radiologists.

Kim et al. [5] developed an automated scheme to facilitate detection of fGGO by extracting ROIs from fixed-size block covering lung regions and classify ROIs by using artificial neural network. Since the sizes of fGGOs in different CT scans could be diverse, the fixed-size block is not appropriate technology for detecting ROIs. Bastawrous et al. [6] presented a template matching method for fGGO detection, and further used artificial neural network to reduce the number of false positive (FR) findings at the expense of low detection sensitivity. Ye et al. [7] reported a high GGO detection sensitivity of 92.3% but a high FR rate of 12.7 per scan by using a voxel-based method with rule-based filtering. In the work of Jacobs et al. [8], a linear discriminant classifier and a GentleBoost classifier were employed to construct a two-stage classification approach for efficiently classifying candidate regions. They achieved a relatively good accuracy: the sensitivity of 73% at one FR per scan.

---

<sup>1</sup> Corresponding Author. Email: lixiabi@bit.edu.cn

In this paper, we propose a novel approach for detecting fGGOs in 2D lung CT images through labeling each region of interests (ROIs) in lung parenchyma as fGGO or non-fGGO. How to extract ROIs in lung parenchyma in 2D lung CT images and how to labeling a ROI as fGGO or non-fGGO are two main problems in the proposed approach. We resort to the techniques of Otsu thresholding and mathematical morphology for solving the first problem. As for the second problem, the solution is based on the Gaussian Mixture Modeling of visual features of fGGOs. A corresponding Bayesian ROI classifier is constructed to identify fGGOs. The features and the parameters in the classifier are learned from the training data. Actually, we develop a genetic algorithm to select the optimal ROI features from CT value histogram (CVH), Histogram of Oriented Gradients (HOG) [9] and Local Binary Pattern (LBP) [10], and apply the Max-Min posterior Pseudo-probabilities (MMP) discriminative learning algorithm [11] to train the classifier parameters. In order to evaluate the effectiveness of the proposed approach, we conducted 5-fold cross-validation experiments on a dataset of 69 thoracic CT scans that contain 70 fGGOs. The experimental results show that our approach is effective and promising.

## 2. ROI EXTRACTION

fGGOs are located in lung parenchyma. So our ROI extraction method is divided into two steps: lung parenchyma segmentation and ROI extraction in lung parenchyma. In this way false positives outside of lung regions can be avoided. We use the techniques of Otsu thresholding and mathematical morphology [12] to complete the two tasks. The Otsu thresholding method is an important image segmentation tool, which has two versions: 1-D [13] and 2-D [14]. We use 1-D Otsu method in lung parenchyma segmentation and 2-D one in ROI extraction in lung parenchyma, respectively.

### 2.1 Lung parenchyma segmentation

Lung parenchyma segmentation procedure is illustrated in Fig. 1 and explained as follows. Our solution of lung parenchyma segmentation is based on the observation that CT values of pixels in lung parenchyma are obviously difference from those in surrounding tissues such as muscle and bone. Thus we try to use 1-D Otsu method to find out an optimal threshold CT value for distinguishing lung parenchyma from other tissues surrounding it. However, the pixels in blank areas in a lung CT image have more apparently different CT values compared with other areas. If we perform 1-D Otsu method on original CT images, we will divide the image into a blank region and another remaining region. We show this problem in Fig. 1b. In order to solve this problem, we truncate the CT value of each pixel to ensure that its magnitude is larger than -900. Consequently, the pixel values in blank areas are made to be close to those in lung parenchyma. But both of them are obviously different from the pixel values in the tissues surrounding lung parenchyma. So the results of 1-D Otsu thresholding on truncated images will be like that illustrated in Fig. 1d.

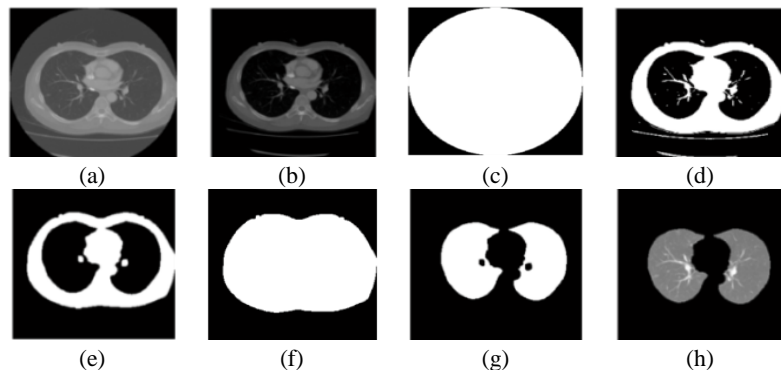


Figure 1. The illustration of lung parenchyma segmentation procedure: (a) original image; (b) CT value truncated image; (c) Otsu thresholding result on Fig. 1a; (d) Otsu thresholding result on Fig. 1b; (e) after opening operation on Fig. 1d; (f) after the first flood-fill operation on Fig. 1e; (g) subtraction of Fig. 1f from Fig. 1e; (h) segmented lung parenchyma after the second flood-fill operation.

However, as shown in Fig. 1d, the lung parenchyma segmented by 1-D Otsu thresholding loses some tissues in it, such as bedplate, blood vessel and etc. The mathematical morphology operation is introduced to repair the deficiency. We perform the opening operation with flat and disk-shaped structuring elements on the result from 1-D Ostu

thresholding. The resultant image is illustrated in Fig. 1e. We then perform twice flood-fill operations to get the final segmentation result. As shown in Fig. 1f, the first flood-fill operation is used to get the region containing lung parenchyma and surrounding tissues. Thus we can obtain the lung parenchyma by subtracting Fig. 1f from Fig. 1e. The second flood-fill operation is used to improve the segmentation result by filling the holes in lung parenchyma region, which can be seen by comparing Fig. 1g and h.

## 2.2 ROI extraction in lung parenchyma

The procedure of ROI extraction in lung parenchyma is illustrated in Fig. 2. Firstly, the 2-D Otsu method is performed on segmented lung parenchyma to get the optimal threshold value for distinguishing the possible imaging sign from the lung parenchyma background. Because 2-D Otsu method considers the spatial relation of pixels, it is better than 1-D Otsu method for extracting small and easy-confused imaging signs. After get the optimal threshold value, the image binarization is conducted. The connected components of white pixels are taken as candidate ROIs, the examples of which can be seen in Fig. 2a. Secondly, the morphology closing operations with flat and disk-shape structuring elements are used to filter too-tiny and useless ROIs. The resultant final result of ROI extraction is illustrated in Fig. 2b, where the red block indicates the ROI corresponding to fGGO.

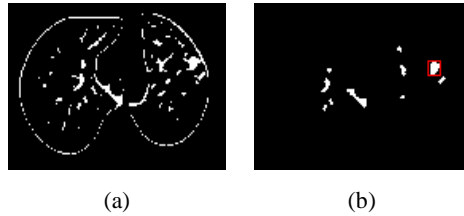


Figure 2. The illustration of the procedure for extracting ROIs in lung parenchyma: (a) 2-D Otsu thresholding result on lung parenchyma; (b) after morphology closing operation on Fig. 2a.

## 3. FGGO IDENTIFICATION

### 3.1 ROI feature extraction and selection

We consider three facets of ROI features, including intensity, shape and texture. They are described by CVH features, HOG features and LBP features, respectively. CVH means the histogram of CT values. The number of bins is set to 40 according to the investigation in [15]. This yields 40 CVH features. HOG feature extraction scheme follow that of Dalal et al. [9]. We normalize a ROI into  $16 \times 16$  pixels and divide it into 4 smaller rectangular cells of  $8 \times 8$  pixels. Then an orientation histogram which contains 9 bins covering a gradient orientation range of  $0^\circ$ -  $180^\circ$  is computed for each cell. In this way 36 HOG features are obtained. For LBP features, we use the LBP operator [10] to compute an integer for each pixel based on the gray values of it and its neighborhood. The neighborhood is denoted by  $(P, R)$  which means we evenly sample  $P$  neighbors on the circle of radius  $R$  around the center pixel. Then the frequency of each integer is figured out on ROI level to get LBP features. Though careful experiments,  $P$  and  $R$  are set to be 4 and 2, respectively. This means we get 16 LBP features

To sum up, we extract total 92 features from each ROI, among which the optimal features for fGGO identification are selected by performing a genetic algorithm (GA) based method on the training data. In our GA-based feature selection method, a chromosome is encoded as a binary bit string. The length of the string is the number of all the candidate features, i.e. 92, in this paper. Each bit in the string corresponds to a feature, where the value 1 indicates that the feature is selected and 0 indicates that the feature is discarded. The fitness function for each chromosome is designed as

$$F = \omega_e \times S_e + \omega_p \times S_p + \omega_f \times L/l \quad (1)$$

where (1)  $S_e$  and  $S_p$  be the sensitivity and specificity of fGGO identification based on the selected features, respectively; (2)  $L$  and  $l$  denote the number of all the candidate features and that of the selected features, respectively; (3)  $\omega_e$ ,  $\omega_p$ , and  $\omega_f$  are corresponding weights for three factors. They are empirically set to be 0.4, 0.4, and 0.2, respectively. Eq. 1 shows that the objective is to find out a combination of features which is compact and leads to accurate fGGO

identification. Accordingly, the conventional GA operations are iterated until the performance improvement is not found in the new generation or the searching generation has reached the preset maximum number. When the iteration stops, the optimal features are obtained according to the best individual.

### 3.2 fGGO modeling and learning

The feature vectors extracted from fGGOs are assumed to be of the distribution of GMM. Let  $\mathbf{x}$  be the feature vector,  $C$  be the fGGO category,  $K$  be the number of Gaussian components in the GMM,  $w_k$ ,  $\mu_k$  and  $\sum_k$  be the weight, the mean, and the covariance matrix of the  $k$ -th Gaussian component, respectively.  $\sum_{k=1}^K w_k = 1$ . Then we have

$$P(\mathbf{x} | C) = \sum_{k=1}^K w_k N(\mathbf{x} | \mu_k, \Sigma_k) \quad (2)$$

where

$$N(\mathbf{x} | \mu_k, \Sigma_k) = (2\pi)^{-\frac{d}{2}} |\Sigma_k|^{-\frac{1}{2}} \exp\left(-\frac{1}{2} (\mathbf{x} - \mu_k)^T \Sigma_k^{-1} (\mathbf{x} - \mu_k)\right) \quad (3)$$

The posterior pseudo-probability of being  $C$  for  $\mathbf{x}$  is computed as [11]

$$f(p(\mathbf{x} | C)) = 1 - \exp(-\lambda p'(\mathbf{x} | C)) \quad (4)$$

where  $\lambda$  and  $t$  are positive numbers. Each ROI will be labeled as fGGO or non-fGGO according to the corresponding value of posterior pseudo-probability.

Before the fGGO identification can be performed, the parameters in the posterior pseudo-probability measure function, i.e.  $\{\lambda, t, w_k, \mu_k, \Sigma_k\}_{k=1}^K$ , need to be decided. To deal with this problem, we firstly use the Expectation-Maximization (EM) algorithm [16] with Minimum Description Length (MDL) [17] criterion on fGGO examples to estimate the GMM parameters  $\{w_k, \mu_k, \Sigma_k\}_{k=1}^K$ . The algorithm is called EM-MDL for short. Here the MDL criterion is used to determine the GMM structure, i.e., the number of Gaussian components. The EM algorithm is used to estimate the parameters in the GMM with specific structure. Then  $\{\lambda, t\}$  is set empirically. We obtain the initial parameters. Finally the MMP learning algorithm [11] is used on both fGGO and non-fGGO examples to revise the initial parameters, including  $\{w_k, \mu_k, \Sigma_k\}_{k=1}^K$  and  $\{\lambda, t\}$ . According to Eq. 3, the posterior pseudo-probabilities take values in  $[0, 1]$ . So the main idea behind MMP learning is to optimize the classifier performance through maximizing posterior pseudo-probabilities towards one for each category and its positive examples, and minimizing those towards zero for each category and its negative examples. The goal is achieved by using the gradient descent optimization strategy.

## 4. EXPERIMENTS

### 4.1 Experimental setup

A dataset of 69 lung CT scans from 38 patients was used to evaluate the effectiveness of the proposed fGGO detection approach. All the lung CT images were taken by slice thickness of 0.5mm and the total slice number for each CT scan ranged from 43 to 131 with an average of 58/scan. There are total 70 fGGOs in the dataset. Their diameters range from 3mm to 16mm. The rectangular ROIs wrapping fGGOs are manually labeled and annotated by us to produce a gold standard.

The 5-fold cross validation experiments of fGGO detection is conducted. The dataset is divided into 5 disjoint subsets by randomly splitting all the available instances for each patient into 5 disjoint sub-sets. In each round of experiments, a subset is used as the test set and the remaining subsets as the training set. We record the average accuracy of fGGO detection from 5 rounds of experiments as the performance measure. In the experiments, the performance of MMP learning is compared with that of EM-MDL and Support Vector Machines (SVM). We used the Sequential Minimal Optimization (SMO) based SVM algorithm in WEKA [18], a machine learning library with java. The four kernel functions for the SMO-SVM algorithm, including Pearson VII Universal Kernel (PUK), Radial Basis Function

(RBF), Polynomial, and Normalized Polynomial, were tested. The PUK leads to the best result reported in the following. Furthermore, in order to evaluate the effectiveness of our GA-based feature selection method, we compared the selected features and the combination of all the candidate features in the experiments.

#### 4.2 Experimental results

The experimental results of fGGO detection on the test set are given in Table 1, where “FP rate” means false positive rate. In Table 1, the data in the column “ROI” is corresponding with the fGGO detection result after performing our ROI extraction method. There are two errors of fGGO detection: false negative and false positive. The error of false negative in ROI extraction is unrecoverable, while the false positive fGGOs could be suppressed in the next fGGO identification stage. So we only concern the fGGO detection sensitivity of our ROI extraction method. The data in other three columns in Table 1 are corresponding with the fGGO detection result after performing our complete detection pipeline, including ROI extraction and fGGO identification, where fGGO\_MMP, fGGO\_EM-MDL, fGGO\_SVM mean the fGGO identification method based on MMP learning, EM-MDL learning and SVM, respectively. Furthermore, “combined” means the combination of all the candidate features, and “selected” means the selected features by using our GA-based method.

As shown in Table 1, our ROI extraction method achieved high sensitivity and our complete fGGO detection approach based on MMP learning achieved acceptable overall accuracy. The data also show that the MMP learning behaved better than EM-MDL learning and SVM, and our GA-based feature selection method is effective.

We carefully explored the reasons for two types of wrong fGGO detection results from our approach: missing fGGOs in the ROI extraction stage and incurring false positive in the fGGO identification stage. They are illustrated in Fig. 3. The hazy and small fGGOs are very easy to be confused with blood vessel surrounding it. This is a main reason for missing error in the ROI extraction stage, which can be seen in the first row of Fig. 3. As for the mis-labeled ROIs in the identification stage, we find the visual appearance of false positive ones are very similar with that of true fGGOs, as shown in the second row of Fig. 3.

Table 1. The average accuracy of fGGO detection on 5 test sub-sets.

Method	ROI	fGGO_MMP		fGGO_EM-MDL		fGGO_SVM	
		combined	selected	combined	selected	combined	selected
Sensitivity	85.7%	78.6%	<b>85.7%</b>	85.7%	85.7%	35.7%	50%
FP Rate	—	2.8	<b>2.5</b>	15.5	12.7	0.7	1.5

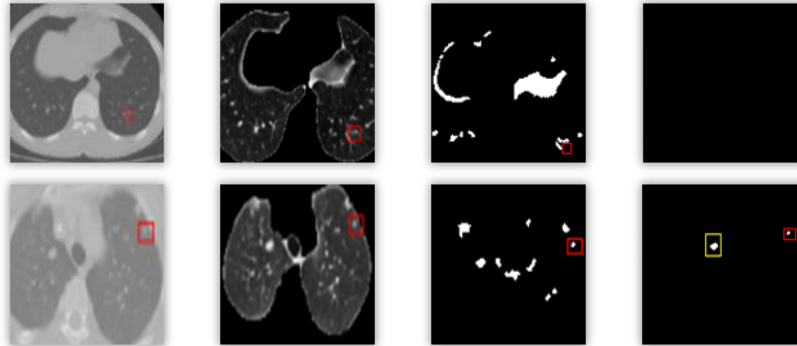


Figure 3. The examples of wrong fGGO detection results: original images and true fGGOs (leftmost), segmented lung parenchyma and extracted ROIs (middle), and the final detection results (rightmost).

## 5. CONCLUSIONS

This paper has proposed a novel approach to focal Ground-glass opacity (fGGO) detection. The main contributions of this paper are summarized as follows. (1) An algorithm based on Otsu thresholding and mathematical morphological operations are developed to segment lung parenchyma and extract regions of interests (ROIs) in the lung parenchyma. (2)

A fGGO identification method is presented based on Gaussian Mixture Modeling (GMM), genetic algorithm-based feature selection and discriminative learning. We show the effectiveness of the proposed approach by conducting 5-fold cross-validation experiments on a dataset of 69 thoracic CT scans that contain 70 fGGOs. The high average detection sensitivity of 85.7% at 2.5 FP per scan was achieved.

In the future, we will try to improve the performance of our approach by carefully investigating the solutions to the errors observed in the experiments. Furthermore, as a framework of the automatic detection of imaging signs, we also want to test the effectiveness of our approach on other categories of imaging signs, such as spiculation, cavity, calcification, and etc.

## REFERENCES

- [1] Austin J.H., Müller N.L., et al., "Glossary of terms for CT of the lung: recommendations of nomenclature committee of the fleischner society," *Radiology*. 200(2), 327-331 (1996).
- [2] Tazi A., Desfemmes-Baleye T., Soler P. et al., "Pulmonary sarcoidosis with a diffuse ground glass pattern on the chest radiograph," *Thorax*. 49, 793-797 (1994).
- [3] Nakata M., Saeki H., et al., "Focal ground-glass opacity detected by low-dose helical CT," *Chest*. 121(5), 1464-1467 (2002).
- [4] Jang H.J., Lee K.S., Kwon O.J., Shim Y.M., Han J., "Bronchioloalveolar carcinoma: focal area of ground-glass attenuation at thin-section CT as an early sign," *Radiology*. 199(2), 485-488 (1996).
- [5] Kim K.G., Goo J.M., et al., "Computer-aided diagnosis of localized ground-glass opacity in the lung at CT: initial experience," *Radiology*. 237(2), 657-661 (2005).
- [6] Bastawrous H.A., Fukumoto T., Nitta N., Tsudagawa M., "Detection of ground glass opacities in lung CT images using Gabor filters and neural networks," *Proceedings of the IEEE Instrumentation and Measurement Technology Conference (IMTC)*, 251-256 (2005).
- [7] Xujiong Ye, Xinyu Lin, Beddoe G., Dehmeshki J., "Efficient computer-aided detection of ground-glass opacity nodules in thoracic CT images," *Proceedings of the 29<sup>th</sup> Annual International Conference of the IEEE EMBS*, 1, 4449-4452 (2007).
- [8] Colin J., Clara I. S., Stefan C. Saur et al, "Computer-Aided Detection of Ground Glass Nodules in Thoracic CT Images Using Shape, Intensity and Context Features," *Proc. MICCAI* 6893, 207-214 (2011).
- [9] Dalal N., Triggs B., "Histograms of oriented gradients for human detection," In *CVPR* 1, 886-893 (2005).
- [10] Ojala T., Pietikainen M., Harwood D., "A comparative study of texture measures with classification based on feature distributions," *Pattern Recognition*. 29(1), 51-59 (1996).
- [11] Xuefeng Chen, Xiabi Liu, Yunde Jia, "Learning Handwritten Digit Recognition by the Max-Min Posterior Pseudo-Probabilities Method," *Proceedings of the 9<sup>th</sup> International Conference on Document Analysis and Recognition (ICDAR 2007)*, 342-346 (2007).
- [12] Boomgaard V.D., Balen V., "Image Transforms Using Bitmapped Binary Images," *Computer Vision, Graphics, and Image Processing: Graphical Models and Image Processing*. 54(3): 254-258 (1992).
- [13] Otsu N., "A threshold selection method from gray-level histogram," *IEEE Transactions on Systems*. 9(1), 62-66 (1979).
- [14] Ying W., Cunxi C., Tong J., Xinhe X., "Segmentation of regions of interest in lung CT images based on 2-D Otsu optimized by genetic algorithm," *IEEE Control and Decision Conference (CCDC'09)*, 5185-5189 (2009).
- [15] Depersinge A., Sage D., Hidki A., Platon A., et al., "Lung tissue classification using wavelet frames," *Proceedings of the 29<sup>th</sup> Annual International Conference of the IEEE EMBS*, 6259-6262 (2007).
- [16] Dempster, A., Laird, N., Rubin, D., "Maximum Likelihood from Incomplete Data via the EM Algorithm," *Journal of the Royal Statistical Society*. 39(1), 1-38 (1977).
- [17] Hansen, M.H., Yu, B., "Model Selection and the Principle of Minimum Description Length," In *Journal of American Statistical Association*. 96(454), 746-774 (2001).
- [18] Geoffrey H., Andrew D., and Ian H.W., "WEKA: a machine learning workbench," *Proceedings of the Second Australia and New Zealand Conference on Intelligent Information Systems*, 357-361 (1994).